


Integrating U-Th, ^{14}C , and ^{210}Pb methods to produce a chronologically reliable isotope record for the Belize River Valley Maya from a low-uranium stalagmite

The Holocene
2019, Vol. 29(7) 1234–1248
© The Author(s) 2019
Article reuse guidelines:
sagepub.com/journals-permissions
DOI: 10.1177/0959683619838047
journals.sagepub.com/home/hol


Pete D Akers,¹  George A Brook,² L Bruce Railsback,³
Alex Cherkinsky,⁴ Fuyuan Liang,⁵ Claire E Ebert,⁶
Julie A Hoggarth,⁷ Jaime J Awe,⁶ Hai Cheng^{8,9}
and R Lawrence Edwards⁹

Abstract

Social and environmental changes had great spatiotemporal variability in the Maya Lowlands during the Classic and Postclassic Periods, and stalagmites promise high-resolution paleoclimate data that can refine our understanding of this complex time. Unfortunately, stalagmites in this region are often difficult to date by U-Th methods because of low initial uranium concentrations. Other dating techniques can be used on such stalagmites, and we present here an age–depth model for BZBT1, a low-uranium stalagmite sampled from Box Tunich cave in the Belize River Valley. This age–depth model dates the growth of BZBT1 to between 400 and 1610 yr BP (340–1550 CE) by combining evidence from U-Th results, radiocarbon dating of both stalagmite CaCO_3 and trapped organic material, and ^{210}Pb dating. The resulting stable isotope record from BZBT1 reveals paleoclimate changes that affected local Maya populations during the Classic and early Postclassic Periods. This record is further refined by isotopically tuning the BZBT1 data with two other regional stalagmite records. Our work offers additional paleoclimate insight into the relationship between the Maya and their environment from a stalagmite that would typically be disregarded for research purposes. Continued research into alternative dating techniques for speleothems can enable additional scientific discovery while promoting speleothem conservation.

Keywords

Maya, paleoclimate, radiocarbon, stable isotopes, stalagmite

Received 8 August 2018; revised manuscript accepted 18 February 2019

Introduction

The lowland Maya of southern Mesoamerica are well known for their achievements in architecture, art, and culture during the Classic Period (1050–1700 yr BP/250–900 CE), as well as their sociopolitical disintegration at the end of the Terminal Classic Period. However, this ‘collapse’ was not a singular event, but rather a mix of violent conquests, orderly abandonments, regime changes, and population migrations extended over more than a century (e.g. Aimers, 2007; Chase and Chase, 2007; Ebert et al., 2014; Iannone, 2014; Turner and Sabloff, 2012). Coinciding with these political and demographic changes were an increasingly variable climate and a series of droughts (e.g. Akers, 2016; Bhat-tacharya et al., 2017; Haug et al., 2003; Hodell et al., 2005; Kennett et al., 2012; Medina-Elizalde and Rohling, 2012; Stahle et al., 2011; Wahl et al., 2014). While the environmental stress from drought is believed to have played a role in the Classic Maya ‘collapse’, the spatiotemporal diversity of both drought itself and the societal responses to drought argue against broad and simple causative conclusions applied across the Maya world. Rather, investigations into the effect of drought on Maya society must be made at the local scale, and this requires precise paleoclimate records with high temporal resolution.

Stalagmites and other speleothems are valued for their highly accurate and precise uranium-thorium disequilibrium series (U-Th)

ages, and recent developments in uranium-lead (U-Pb) dating have only added to their appeal (Dorale et al., 2004; Fairchild and Baker, 2012; Hellstrom and Pickering, 2015; Woodhead and Pickering, 2012). Speleothems also preserve multiple environmental proxies,

¹Institut des Géosciences de l'Environnement, CNRS, IRD, Université Grenoble Alpes, Grenoble, France

²Department of Geography, University of Georgia, Athens, GA, USA

³Department of Geology, University of Georgia, Athens, GA, USA

⁴Center for Applied Isotope Studies, University of Georgia, Athens, GA, USA

⁵Department of Geography, Western Illinois University, Macomb, IL, USA

⁶Department of Anthropology, Northern Arizona University, Flagstaff, AZ, USA

⁷Department of Anthropology and Institute of Archaeology, Baylor University, Waco, TX, USA

⁸College of Global Environmental Change, Xi'an Jiaotong University, Xi'an, P.R. China

⁹Department of Geology and Geophysics, University of Minnesota, Minneapolis, MN, USA

Corresponding author:

Pete D Akers, Institut des Géosciences de l'Environnement, CNRS, IRD, Université Grenoble Alpes, 38000 Grenoble, France.
Email: pete.akers@univ-grenoble-alpes.fr

including stable isotopes (Lachniet, 2009; McDermott, 2004; Wong and Breecker, 2015), organic compounds (e.g. Blyth et al., 2016; McGarry and Baker, 2000), and petrographic changes (e.g. Railsback et al., 2013). However, many speleothems that hold valuable paleoenvironmental information are difficult or impossible to date by U-Th methods because of low uranium concentrations, excess detrital contamination, or open system geochemical behavior (Bajo et al., 2016; Blyth et al., 2017; Fensterer et al., 2010; Lachniet et al., 2012). Alternative methods of dating speleothems can potentially produce successful paleoenvironmental reconstructions from specimens otherwise ignored or discarded, while also offering new opportunities in regions currently underutilized because of perceived dating difficulties.

Western Belize has extensive karst and cave systems, but stalagmites from this region are often difficult to date with standard U-Th methods (Akers, 2011; Akers et al., 2016; Webster et al., 2007). Despite this challenge, stalagmite records are needed to fill spatiotemporal gaps in climate history for archaeologists working in the region (Douglas et al., 2016). We present here a chronology and paleoenvironmental record for stalagmite BZBT1 from Box Tunich cave in the Belize River Valley of western Belize. Our chronology dates the growth of the stalagmite to 400–1610 yr BP (340–1550 CE). All ages are reported as calendar years BP (yr BP, where BP is 1950 CE) unless otherwise noted. An initial radiometric age–depth model for BZBT1 combines evidence from U-Th, radiocarbon (both of CaCO₃ and trapped organic material (OM)), and ²¹⁰Pb dating. This model was ‘tuned’ by correlating the BZBT1 oxygen and carbon stable isotope ratio ($\delta^{18}\text{O}$ and $\delta^{13}\text{C}$, respectively) time series with two other regional stalagmite isotope records and making necessary adjustments. The resulting tuned chronologies are very similar to our initial radiometric model and reveal a paleoenvironmental history for the western Belize River Valley, an area previously lacking such information. The methods we used in developing the BZBT1 chronology may help other researchers who face similar stalagmite dating difficulties.

BZBT1 description

BZBT1 is a 93 mm tall stalagmite that was collected on May 11, 2010, in a middle passage of Box Tunich Cave, Cayo District, Belize (17.090°N 88.947°W, 335 m a.s.l.). Box Tunich is located in a karst upland at the intersection of the Belize River Valley to the north and the Mountain Pine Ridge and Maya Mountains to the south (Figure 1). Annual precipitation is high (2100 mm) and largely falls in the wet season (Jun–Oct), while local vegetation consists of evergreen broadleaved forest with some leaf drop in the dry season (Akers et al., 2016; Penn et al., 2004). There are several major and minor Maya sites within 50 km of the cave, particularly on the Vaca Plateau to the southwest and throughout the Belize River Valley (Awe et al., 2014; Chase et al., 2014; Ebert et al., 2016).

Although the surface directly above Box Tunich does not have clear evidence of prehistoric modification, the 20 km² area surrounding the cave contains over 200 architectural platforms, at least 14 km of terracing, and a minor population center (Figure 1) as revealed by lidar (Section S1, available online). In addition, numerous ceramic vessels and other artifacts placed throughout Box Tunich demonstrate that it was ritually visited by the Maya during the Classic Period. Even though the immediate area around Box Tunich was not heavily modified, the significant Maya presence in the local region makes it likely that the environment near the cave was used in some fashion for food and resources.

The natural entrance to Box Tunich is approximately 2 m high and 1 m wide on a steep hillside of brecciated limestone, and the cave today has been partly developed for tourism. The cave contains a large number of speleothems (particularly stalactites and

flowstones), but stalagmites suitable for paleoclimate work are rare. BZBT1 grew in a small alcove approximately 5 m above the current cave floor along a well-decorated wall. The cave is warm and humid, with a temperature of 24.8°C and 79% relative humidity in the chamber during midday at the time of collection. These conditions in Box Tunich are slightly warmer and drier than those in nearby caves (Akers, 2011), which suggests that BZBT1’s chamber has relatively more ventilation and outside air exchange.

At the time of collection, the outermost layer of BZBT1 was largely clean of detritus, but there was no clear evidence whether BZBT1 was actively growing or not. While stalagmite activity can be notoriously difficult to judge from appearance alone, BZBT1 did not share the fresh appearance of a brilliant white active flowstone and drapery growing less than 1 m away. When cut, BZBT1 revealed multiple calcite fabric types visible to the naked eye and in thin section (Figure 2). The lowest 13 mm comprises a very dense, massive, and columnar calcite. This dense calcite is translucent and thus appears dark to the naked eye. In contrast, most of the stalagmite above this is a porous, braided calcite that appears white to the naked eye because of light scattering and reflection. This braided fabric also has very fine laminae of slightly denser calcite at varying intervals and is interrupted by at least four thicker laminae of dense, translucent calcite. A fine opaque detrital material of indistinguishable grains (clay to fine silt) is observed at several significant petrographic boundaries. Where present, this detritus is distributed thinly and evenly across the laminal surface.

The uppermost 20 mm of BZBT1 is more irregular than the portion below, with wavy laminae that only extend about two-thirds of the way down the flanks. This depositional regime shift is associated with a major petrographic boundary, where a Type L surface (Railsback et al., 2013) is capped by a dense calcite layer that extends down the stalagmite flanks (Figure 2(c)). At the fabric boundary, there is a thick detrital layer and loss of polarized optical continuity, suggesting a significant environmental change across the boundary and a possible growth hiatus. Two additional Type E petrographic surfaces (Railsback et al., 2013) are present at 80 and 87 mm, and growth hiatuses are also possible here where lamina were eroded (Section S2, available online).

Developing stalagmite chronologies

U-Th dating

Under ideal circumstances, U-Th dating can produce age–depth models with very low uncertainties (<5%) that extend back over 500,000 years, and U-Pb dating has shown promise for accurate dating to at least 8 Ma (Cheng et al., 2000; Shen et al., 2002; Woodhead and Pickering, 2012). This enables paleoenvironmental reconstructions well beyond the temporal limit of radiocarbon dating, while also avoiding accuracy and uncertainty issues inherent in radiocarbon calibration curves. For optimal results, speleothems must act as a closed system for uranium and lack diagenesis (Bajo et al., 2016; Lachniet et al., 2012). However, even speleothems that approximate a closed system can produce disappointing U-Th results.

A closed-system speleothem may prove difficult to date by U-Th methods, if it is contaminated with detrital ²³⁰Th (common in ‘dirty’ stalagmites) (e.g. Blyth et al., 2017) or if it has a very low initial ²³⁸U concentration (e.g. Fensterer et al., 2010). Difficulties caused by detrital ²³⁰Th contamination can be mitigated somewhat by isochron dating techniques that better estimate initial ²³⁰Th concentrations (Dorale et al., 2004) and/or by selectively taking age samples from ‘cleaner’ laminae (e.g. Akers, 2016). In addition, individual speleothems within a single cave often exhibit high variability in mean detrital content, and it may

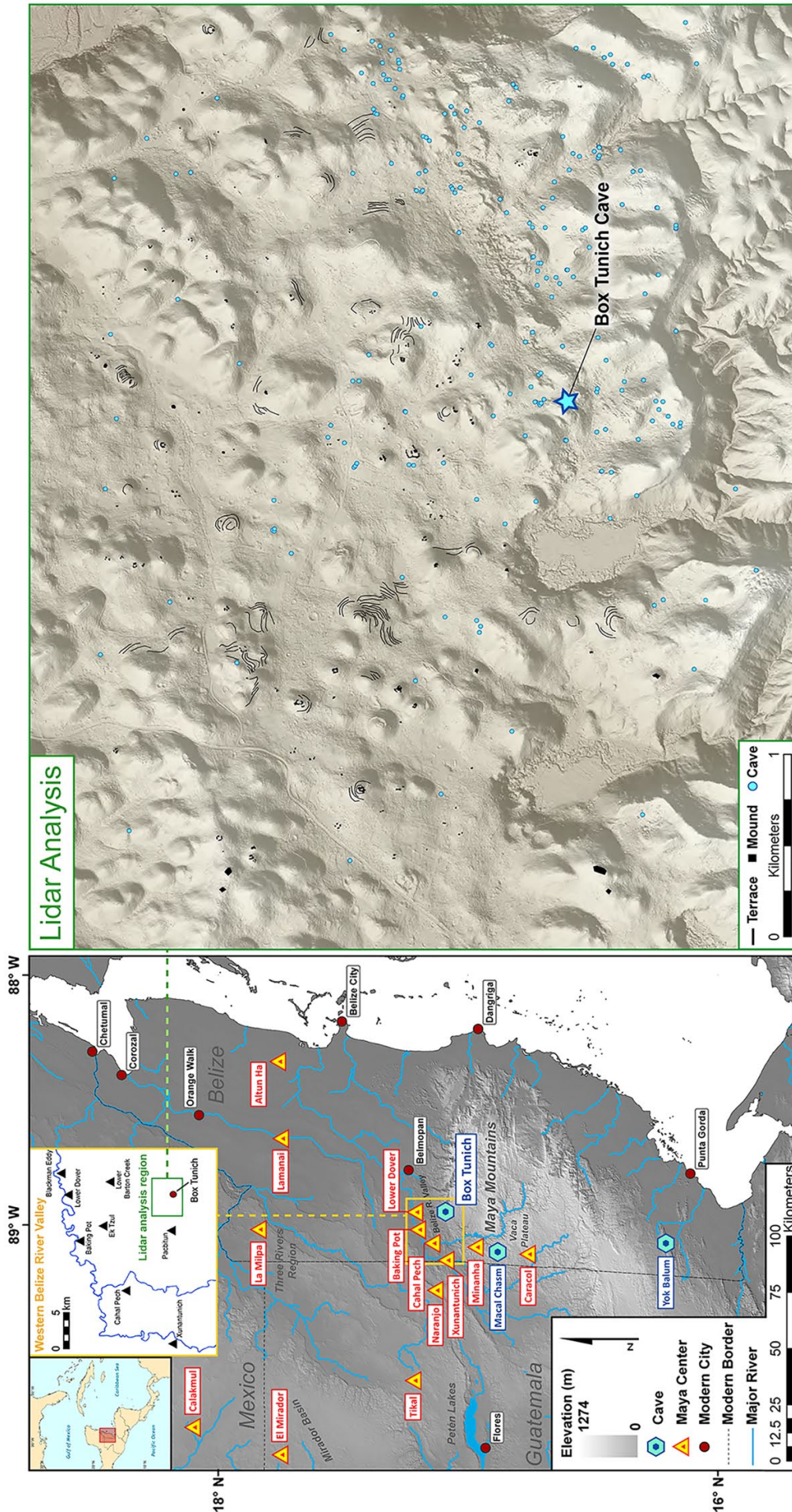


Figure 1. Locations of important regional Classic Maya centers relative to Box Tunich and other caves mentioned in the text. Lidar analysis of the local area around Box Tunich (highlighted at right) shows Maya mounds and terracing, as well as dozens of additional caves (Section S1, available online).

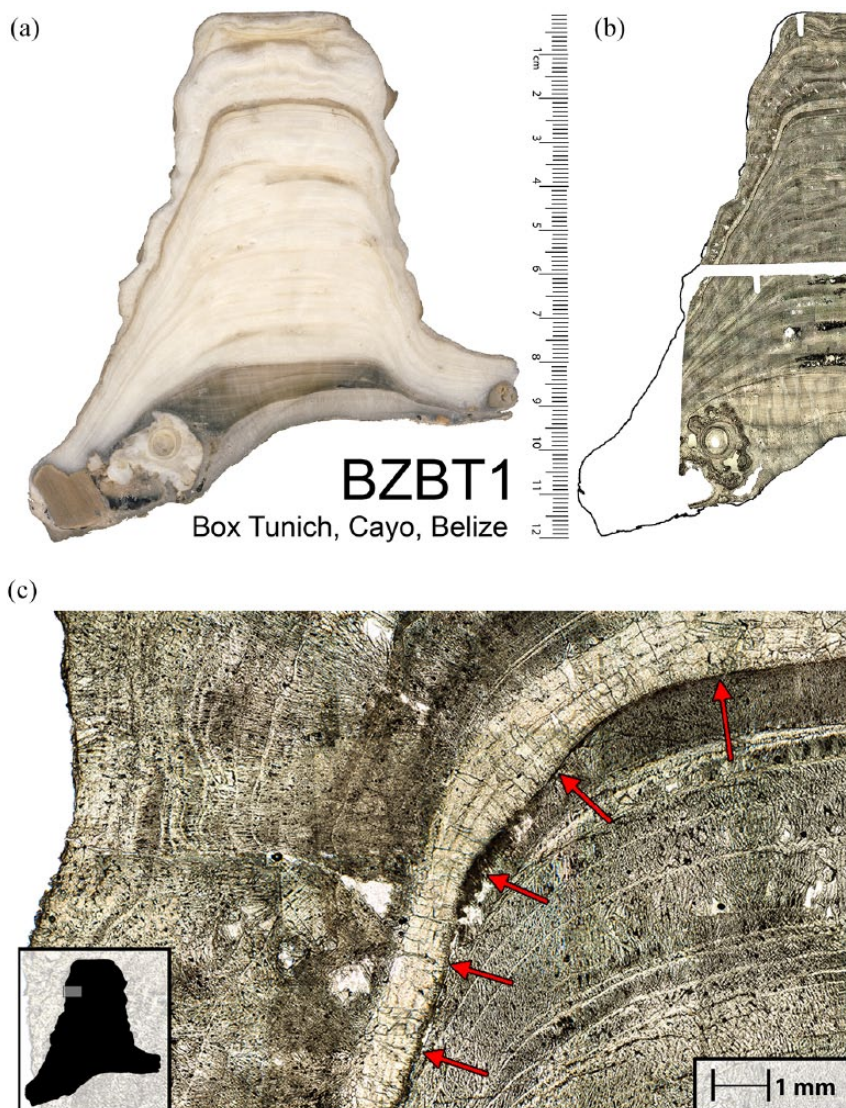


Figure 2. (a) Natural light image of a polished half of stalagmite BZBT1. Dense translucent calcite appears darker while the lighter zones consist of a braided calcite fabric. (b) Composite of petrographic thin section images taken through a microscope. In contrast to the natural light image, dense calcite appears as the more even and lighter layers while braided zones appear granular and darker. The black regions in the lower half of the petrographic image are artifacts from the thin section slide mounting process. (c) Detail of the petrographic composite showing the fabric change and prominent detrital layer at 20 mm (arrows).

be possible to sample alternative speleothems that are not quite so ‘dirty’ and can be dated more precisely.

In contrast, low initial uranium concentrations and their associated dating problems can be endemic across speleothems in entire cave systems or geographic regions (Adkins et al., 2013; Akers, 2011; Kennett et al., 2012), particularly with calcite stalagmites. Even in regions where uranium levels are relatively high, some speleothems may suffer from low ^{238}U concentrations because of individual hydrologic and weathering conditions. Pre-sampling speleothems in situ for uranium content prior to full removal can identify specimens with the most dating potential and minimize ‘wasteful’ collection (Scroxton et al., 2016). In addition, sampling can focus on stalagmites containing abundant aragonite (e.g. Jamieson et al., 2016; Kennett et al., 2012), as uranium is preferentially incorporated into aragonite compared with calcite (Wassenburg et al., 2016). However, a need to date low-uranium speleothems still exists for such speleothems that have already been collected and archived, as well as for regions where no accessible specimen suitable for U-Th dating exists.

In 2010, we collected seven stalagmites from five caves in a study region within 20 km of Box Tunich, but all stalagmites sampled in this region were purely calcite. Five stalagmites

contained <10 ppb ^{238}U , and the other two contained <50 ppb ^{238}U . These very low concentrations made U-Th dating by standard means unfeasible. Although two additional caves in the broader western Belize region have contained calcite stalagmites that were successfully dated by U-Th (Macal Chasm, Cayo District (Akers et al., 2016; Webster et al., 2007) and Jose Cueva, Cayo District (unpublished data)), uranium concentrations in these stalagmites were still low and produced less than ideal age precision. As a result, we explored alternative potential methods of dating stalagmites already in our possession rather than attempting additional collection.

Radiocarbon dating

The first ages for speleothems were obtained by radiocarbon dating (Broecker et al., 1960; Hendy and Wilson, 1968). However, these early studies recognized that dating speleothem CaCO_3 produces ages that are older than the actual date of deposition because of incorporation of ‘dead carbon’ from the limestone bedrock (no ^{14}C) and/or aged soil organic matter (less ^{14}C than modern carbon). Thus, the radiocarbon age of speleothem CaCO_3 is a function of the balance between ‘live’ atmospheric carbon and ‘dead’

bedrock/soil sources (Goslar et al., 2000; Lechleitner et al., 2016a). In addition, stalagmites that grew after ~1950 CE will be affected by the increased atmospheric ^{14}C from nuclear testing and often have modern carbon percentages greater than 100% (e.g. Genty et al., 1998; Hodge et al., 2011; Lechleitner et al., 2016a).

To obtain an accurate age for speleothem CaCO_3 , it is typically necessary to correct the dead carbon fraction (DCF) before calibration. However, recent studies of speleothems dated by both radiocarbon and U-Th methods show that the DCF can often vary during the growth of a speleothem (Cai et al., 2005; Genty et al., 1999; Griffiths et al., 2012; Lechleitner et al., 2016a, 2016b; Noronha et al., 2014), and no single DCF correction can be applied to such stalagmites. In particular, changes in the local hydrological system can alter the DCF by shifting from a more open system during wetter conditions (and thus higher DCF) to a more closed system during drier conditions (and thus lower DCF) (Fohlmeister et al., 2010; Griffiths et al., 2012; Lechleitner et al., 2016a).

U-Th ages (calendar yr BP) for five stalagmites from Belize, China, and Flores, Indonesia are 0–2000 years younger than equivalent CaCO_3 radiocarbon ages (^{14}C yr), with most 600–1500 years younger (Cai et al., 2005; Griffiths et al., 2012; Li et al., 2017; Webster et al., 2007). In the Belize stalagmite MC01, six of eight radiocarbon ages are 580–940 years older than U-Th ages for the same CaCO_3 (Webster et al., 2007). An alternative approach (Lechleitner et al., 2016b) can produce robust chronologies by calculating a best fit growth rate between stalagmite CaCO_3 radiocarbon data and the variability of atmospheric ^{14}C . However, this approach requires a relatively stable DCF and growth rate over time, and results from BZBT1 do not support either of these assumptions.

Dating OM trapped within speleothem CaCO_3 by radiocarbon is an alternative to dating the CaCO_3 itself. This approach has been successfully applied to stromatolites (Brook et al., 2013) and organic-rich speleothems (Blyth et al., 2017; Borsato et al., 2000), but is rarely utilized because of the superiority of U-Th dating as well as the low OM content of most speleothems (Blyth et al., 2017). In a stalagmite, OM may be included in a variety of ways (Blyth et al., 2016; McGarry and Caseldine, 2004; Wynn and Brocks, 2014), including flushing of soluble organic molecules and particles along the drip water path, settling of fine eolian or flood sediments on the stalagmite surface, animal droppings, and microbial/algal growths. In rarer cases, larger faunal remains, such as snails, mites, or bats, may be encased by CaCO_3 (e.g. Czaplewski et al., 2003).

Trapped OM can range in age from modern to multiple centuries, at the time it is included in a stalagmite (Blyth et al., 2017; Genty et al., 2011; McGarry and Caseldine, 2004; Trumbore, 1993, 2000). While turnover rates of OM are generally faster in tropical soils, some organic fractions can persist much longer at depth (Lechleitner et al., 2016a; Trumbore, 2000). Previous studies in cooler, non-tropical climates that favor longer OM preservation suggest that OM in stalagmites is typically 300–1000 years old when trapped (Blyth et al., 2017; Genty et al., 2011). At Yok Balum cave in Belize, soil OM is less than 50 years old (Lechleitner et al., 2016a), but much older OM has been found in other tropical and subtropical soils (Griffiths et al., 2012; Meyer et al., 2014; Noronha et al., 2015).

Petrographic examination of a speleothem can help determine the identity and source of trapped OM (Akers, 2016; Blyth et al., 2017; Denniston and Luetscher, 2017; Railsback et al., 1999). Observations of larger detrital grains or thick deposits would suggest a water-borne origin, potentially in floods, while a thin coating of indistinguishable detrital grains may result from eolian deposition. Faunal remains can often be identified easily under the microscope, and direct deposits of guano or insect frass are

noticeable by their uneven distribution across individual layers. Changes in crystal fabric type and evidence of erosion or growth hiatuses can also add contextual clues to the environmental history of trapped OM (e.g. Borsato et al., 2015; Railsback et al., 2013).

^{210}Pb dating

With a half-life of 22.23 years, ^{210}Pb has been used principally to date clastic sediments less than 100 years old (Appleby, 1998; Appleby et al., 1997; Sanchez-Cabeza and Ruiz-Fernández, 2012; Walling, 1999) and more rarely speleothems (e.g. Baskaran and Iliffe, 1993; Tanahara et al., 1998; Webster et al., 2007). When applied to speleothems, this method is typically used to estimate recent growth rates or determine if a stalagmite was recently active.

Isotope tuning and interpretation

Chronological tuning uses a well-dated time series to adjust and improve age accuracy and/or precision in a less well-dated time series, such as applying astronomical cycles of Earth's orbit to ocean and ice core records (e.g. Martinson et al., 1987; Shackleton, 2000; Westerhold et al., 2008). In recent years, the high chronological accuracy of stalagmite isotope time series has been used to establish reliable ages for key climatological events that can be transferred to other records (e.g. Drysdale et al., 2007; Genty et al., 2003; Wang et al., 2001). Although different stalagmites will have different isotope means and ranges (Akers, 2016; Denniston et al., 1999; Hartmann and Baker, 2017; Markowska et al., 2016), extreme environmental changes produce prominent excursions in stalagmite isotopes that can be identified and correlated across records. This concept is well suited to Mesoamerica, where extreme regional climate events (particularly droughts) are captured across diverse proxy records (e.g. Akers et al., 2016; Kennett et al., 2012; Wahl et al., 2014).

The interpretation of stable isotopes in stalagmites is complex, and the dominant environmental controls can change dramatically from cave to cave or even between stalagmites within a single cave. Generally, speleothem $\delta^{18}\text{O}$ is assumed to reflect the $\delta^{18}\text{O}$ of local precipitation, although this can be significantly altered by isotopic fractionation from evaporation and degassing at all points along the water's path from the cloud to the cave. In addition, precipitation may be mixed with existing water during transit through the soil, epikarst, and overlying bedrock, resulting in cave drip water with a temporally aggregated $\delta^{18}\text{O}$ value ranging from days to months (Lachniet, 2009; McDermott, 2004; Wong and Brecker, 2015).

Speleothem $\delta^{13}\text{C}$, in contrast, is generally assumed to reflect the $\delta^{13}\text{C}$ of local soil organic matter, which itself is influenced by vegetation photosynthetic pathways, vegetative cover, and soil productivity/activity. Like $\delta^{18}\text{O}$, this value of $\delta^{13}\text{C}$ may also be significantly altered by isotopic fractionation because of CO_2 degassing and CaCO_3 deposition occurring before the drip water reaches the speleothem (Banner et al., 2007; Dreybrodt and Scholz, 2011; Meyer et al., 2014; Noronha et al., 2015; Wong and Brecker, 2015).

The isotopes of speleothems from caves in seasonally wet tropical climates are typically interpreted as higher $\delta^{18}\text{O}$ and $\delta^{13}\text{C}$ values representing drier conditions. A drying climate may drive isotopic values higher through multiple factors that often interact synergistically, including the negative 'amount effect' observed in tropical precipitation, the reduction in vegetative cover and productivity, and kinetic fractionation effects driven by precipitation-induced changes in cave humidity and pCO_2 (Akers et al., 2016; Kennett et al., 2012; Moquet et al., 2016; Pu et al., 2016). The isotopes in BZBT1 are interpreted here in such a manner, where higher $\delta^{18}\text{O}$ and $\delta^{13}\text{C}$ values reflect drier conditions and lower values reflect wetter conditions.

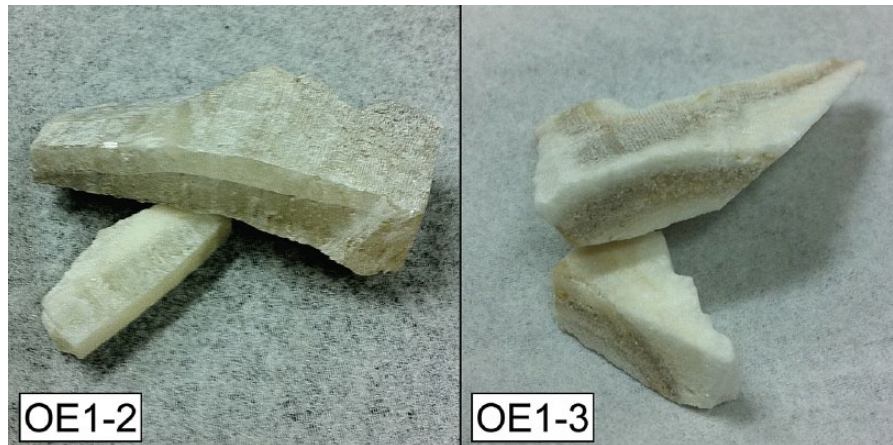


Figure 3. Two of the samples taken for radiocarbon dating of trapped organic material. Scales are different in each photograph, but each large piece is roughly 3–6 cm wide and 1–2 cm thick.

Methods

To date the growth history of BZBT1, samples were collected separately for U-Th dating, radiocarbon dating of OM, radiocarbon dating of CaCO_3 , and ^{210}Pb dating. Nine ~150 mg U-Th samples of calcite powder were drilled at points of presumed low detrital content along the growth axis of BZBT1. These were analyzed at the Minnesota Isotope Laboratory in the University of Minnesota using inductively coupled plasma mass spectrometry (ICP-MS, Neptune) according to the method described by Edwards et al. (1987) and Shen et al. (2002). Calculations used half-lives determined by Cheng et al. (2000), and ages were reported with analytical errors of two standard deviations of the mean.

Large (1–5 g) pieces of the stalagmite were cut for OM radiocarbon dating with a diamond blade band saw (Figure 3) in order to recover enough OM for analysis. Nine sites were sampled: six in detritus-rich layers and three at prominent petrographic boundaries with no visible detritus, but which might favor OM accumulation because of changing environmental conditions. Cut samples extended 2–5 mm above and below targeted layers parallel to growth.

Samples were analyzed at the Center for Applied Isotope Studies (CAIS), University of Georgia. The sample pieces were cleaned to remove external contaminants and then treated with HCl to dissolve the CaCO_3 . After dissolution, samples were heated (for more effective removal of resistant carbonates) with 1 N HCl for 1 h at 80°C. The residual material was washed with deionized water until the pH = 6 and dried at 60°C. If OM was present, the cleaned samples were combusted at 900°C in evacuated/sealed ampoules in the presence of CuO and the resulting CO_2 was catalytically converted to graphite (Vogel et al., 1984). Graphite $^{14}\text{C}/^{13}\text{C}$ ratios were measured with a 0.5 MeV accelerator mass spectrometer (AMS) and compared with the Oxalic Acid I (NBS SRM 4990) standard. Background samples were anthracite sharing the same sample sizes and treatment. Methods used to extract OM from BZBT1 capture only the solid material trapped in the stalagmite and are not designed to include dissolved OM, which is often the oldest OM fraction (Trumbore, 2000). Ages were calibrated using IntCal13 and the Calib7.10 program (Stuiver and Reimer, 1993).

The $\delta^{13}\text{C}$ values of the extracted material were measured separately using an EA-MS system Delta-V spectrometer. Sample data were isotopically standardized to $\delta^{13}\text{C} = -25\text{‰}$ prior to radiocarbon age calculation. All extracted OM $\delta^{13}\text{C}$ values are relative to the Vienna Pee Dee Belemnite (V-PDB) standard with an error of less than 0.2‰.

Nine 20 mg samples of CaCO_3 powder were drilled at regular intervals along the growth axis of BZBT1, although the uppermost sample was drilled from the exposed apex surface. After

reaction with 100% H_3PO_4 at 75°C for 1 h to recover CO_2 , these samples were AMS radiocarbon dated at CAIS as described previously. The $\delta^{13}\text{C}$ values of the CaCO_3 were measured separately using a conventional stable isotope ratio MAT-252 mass spectrometer. All CaCO_3 $\delta^{13}\text{C}$ values are relative to V-PDB with an error of less than 0.1‰.

Samples were collected from the youngest layers of BZBT1 for ^{210}Pb dating to estimate when the stalagmite stopped growing and the latest growth rate. The top 30 mm of BZBT1 was cut into four sequential pieces (0–1, 1–11, 11–18, and 18–30 mm), which were analyzed at the University of Delaware by methods described by Webster et al. (2007).

To develop a stable oxygen and carbon isotope record for BZBT1, 188 samples were drilled along the growth axis at 500 μm intervals using a computer-controlled micromill. The samples were analyzed at the Alabama Stable Isotope Laboratory of the University of Alabama, Tuscaloosa, on a Gasbench II and Delta Plus isotope ratio mass spectrometer using methods described by Lambert and Aharon (2011).

Results

U-Th dating

The U-Th samples had very low ^{238}U concentrations (3.8–49.1 ppb) and low to moderate ^{232}Th concentrations (66–1090 ppt) (Table S1, available online). Two samples (U1-1 and U1-5B) produced anomalously old ages with high uncertainty, but the remaining samples are clustered between 1000 and 2300 yr BP. While the U-Th ages are neither precise nor accurate enough to construct an age–depth model on their own, the general agreement in age range suggests that they are useful in identifying the likely period of stalagmite growth.

Radiocarbon dating of OM

Five of the nine samples produced enough OM for dating and $\delta^{13}\text{C}$ analysis, and the sixth produced enough for a $\delta^{13}\text{C}$ measurement (Table S2, available online). All six successful samples were from layers with visible detritus, and the six OM $\delta^{13}\text{C}$ values range from -21.5‰ to -24.9‰ (Table S3, available online). In contrast, the three samples with insufficient OM for dating or $\delta^{13}\text{C}$ analysis were from sites with no visible detritus.

After calibration, the five ages range from 1700 yr BP at the base to 900 yr BP at 20 mm below the apex. Four of the five ages are in stratigraphic order, but the age at 87 mm is approximately 400 years younger than the general trend of the other four ages. This deviant age was later found to contradict the trends and age

conclusions from the other dating techniques as well. With the very small amounts of OM being dated in each sample, it is quite possible that this sample was contaminated by modern carbon and it was not considered further.

Radiocarbon dating of CaCO_3

The CaCO_3 sample from the exposed apex of BZBT1 produced a very young age of 350 ^{14}C yr BP and a very high $\delta^{13}\text{C}$ value of -2.6% . This age suggests the inclusion of modern ‘bomb carbon’ in the uppermost layers and/or a very low DCF (Lechleitner et al., 2016a, 2016b). As this sample contained material from the exposed surface, it is unclear whether the modern carbon originated in the stalagmite CaCO_3 or was post-growth surface contamination. Combined with a general lack of other chronological support for growth up to modern day, this age was largely not considered in later chronological analysis.

The remaining eight CaCO_3 samples date between 1150 and 2100 ^{14}C yr BP (Table S3, available online). However, the ages are not all in stratigraphic order likely because of small variations in the DCF among the samples. The eight samples have $\delta^{13}\text{C}$ values between -5.6% and -10.6% , which fall within the $\delta^{13}\text{C}$ range observed in the BZBT1 stable isotope data and within the range of data from other Belize stalagmites (Akers et al., 2016; Kennett et al., 2012; Lechleitner et al., 2016a).

Lead-210 dating

Very low ^{210}Pb activity (~ 10 mBq/g) was detected in the uppermost sample from the top millimeter of BZBT1. Although the activity was low, a distinct photopeak was observed and the activity passed a test of significance. The sample was counted for 3 days on two separate occasions with the same result, suggesting that this uppermost sample is less than a century old. However, there was no ^{210}Pb activity in the three deeper samples which indicates that these samples are more than 100 years old. All other ^{238}U daughters were below or just barely above minimum detection limits in all samples.

Although the uppermost ^{210}Pb sample was treated to reduce potential contamination, the process of obtaining this small sample from only the top 1 mm of BZBT1 introduced a relatively high risk of modern contamination. The very low activity of the sample, combined with a lack of any activity in the next lowest sample, raises some doubt as to whether the signal comes from ^{210}Pb within BZBT1 or rather later surface contamination. Similar to the uppermost CaCO_3 sample, this result was largely not considered in later chronological analysis (although the potential that these two samples are valid and represent modern growth is discussed later).

Stable isotopes

The stable isotope values vary considerably, but the $\delta^{18}\text{O}$ and $\delta^{13}\text{C}$ time series are similar (Spearman correlation: $+0.76$) with corresponding high and low peaks (Figure 5). The $\delta^{18}\text{O}$ and $\delta^{13}\text{C}$ values range from -1.9% to -6.6% (median: -3.6%) and from -2.0% to -12.3% (median: -10.0%), respectively. Above the possible growth hiatus at 20 mm, $\delta^{18}\text{O}$ and $\delta^{13}\text{C}$ values increase steadily toward the apex. This trend, and the irregular petrography in this interval, may indicate steadily decreasing drip water until growth ceased.

Radiometric chronology for BZBT1

Chronological model assumptions

The radiometric age data obtained for BZBT1 are shown in Figure 4. With these data, we used the following assumptions to develop an initial chronology.

- Growth over the limited time during which BZBT1 was active can be approximated by one or more straight lines of constant growth rate.

While the actual growth rate of a stalagmite can vary substantially over time and often include growth hiatuses (e.g. Banner et al., 2007; Matthey et al., 2010; Railsback et al., 2013), linear interpolation between ages offers a well-established, if somewhat crude, approximation of a stalagmite’s age–depth relationship. Such linear modeling is employed here with the acknowledgment that the age–depth model is only an initial rough estimate and has a very wide uncertainty.

- Despite low uranium levels in all U-Th samples, some U-Th ages may provide useful chronological data. We particularly favor ages with one or more of the following: higher ^{238}U level, higher $^{230}\text{Th}/^{232}\text{Th}$ ratio, lower ^{232}Th level, and lower age uncertainty.

While the U-Th ages are too uncertain to produce a chronology alone, the relatively tight clustering of many ages suggests that their data reflect partly robust results. Five U-Th ages have part or all of their age uncertainty range younger than CaCO_3 ages of similar depths, as expected for valid U-Th data. Because low-uranium stalagmites are impacted greater by detrital ^{230}Th , we expect any errors introduced by thorium to skew ages older. Thus, we expect the younger ages to be the most useful, and we favor the younger portion of uncertainty ranges.

- The OM recovered from the stalagmite is predominately derived from surface vegetation that was modern or only a few decades old when trapped, and thus calibrated OM radiocarbon ages provide realistic information on the age of stalagmite deposition at the sample depths. For simplicity, we assumed all OM recovered was modern at the time of entrapment.

Petrographic examination of BZBT1 supports flushing of soil material along the drip water path as a viable source of the visible detritus. The large natural entrance and evidence of ventilation in Box Tunich also supports a possible eolian and/or faunal origin of OM, but the even distribution of detritus along petrographic boundaries in BZBT1 argues against discrete guano or frass deposition. Flooding is not a likely source of BZBT1’s detritus, since BZBT1’s cave chamber has no active or remnant stream as well as no visible flood deposits on the walls or speleothems. In addition, BZBT1 was located 5 m above the current cave floor and the local karst environment does not seem likely to support cave flooding events of a magnitude able to reach BZBT1. Thus, it appears that the trapped OM was likely transferred onto the stalagmite either through drip flushing or airborne settling.

The $\delta^{13}\text{C}$ values of the material extracted from BZBT1 for radiocarbon dating (-21% to -25%) support an organic source consistent with partly disturbed to undisturbed tropical forest soils and vegetation (Farquhar et al., 1989; O’Leary, 1988; Powers and Veldkamp, 2005). Without a systematic study of local soil and epikarst characteristics (unfortunately unavailable for the Box Tunich site), we lack local guidance on applying an age correction using observed soil residence times. The assumption of modern/near-modern OM at the time of entrapment assumes a thin and young soil similar to Yok Balum (Lechleitner et al., 2016a), but we do acknowledge a significant risk of pre-inclusion age underestimation. We also reiterate that this modern estimate is being used for an initial approximate chronology, and refinement with isotope tuning may support adjustment of this assumption to represent much older OM.

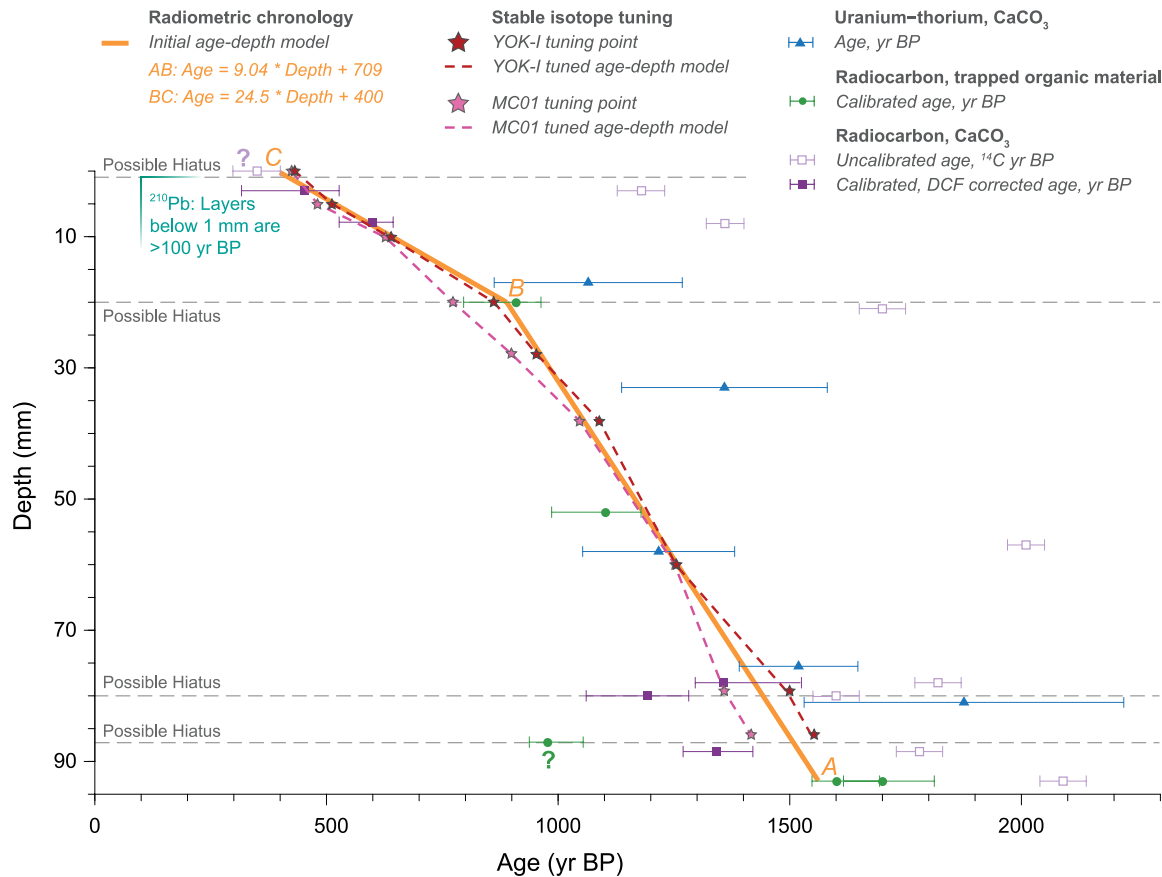


Figure 4. Age data and age-depth models for BZBT1. All ages are plotted with 2σ uncertainty and as calendar years, with the exception of the uncalibrated CaCO_3 radiocarbon ages that are plotted as ^{14}C years. The DCF corrections for the calibrated CaCO_3 radiocarbon ages (0–75 mm: 750 ^{14}C yr; 75–93 mm: 350 ^{14}C yr) are based on observed offsets between paired CaCO_3 and OM radiocarbon ages. Although calibrated CaCO_3 radiocarbon ages are plotted with 2σ calibration ranges, the accuracy uncertainty in these ages should be considered to be greater due to DCF variability and possible pre-trapped aging of OM. Tuning point ages and age models are derived from isotope matching detailed in Table 1. Question marks indicate ages that were not considered in age modeling.

That said, the most robust U-Th ages agree relatively well with OM radiocarbon ages when assuming the OM was modern, as four of the U-Th ages overlap within 2σ uncertainty with the age–depth trend for the four accepted OM ages. If the OM was significantly older than modern, prior to incorporation in BZBT1, the OM ages would shift to be much younger than all the U-Th ages. In addition, the OM ages both fall within a narrow age range and increase in age with depth (with the exception of the OM age at 87 mm). If old carbon was a significant component of the OM, the OM ages would likely have much higher age variance and include some radically older ages (e.g. the cave sediment in Polk et al., 2007).

- Stalagmite CaCO_3 radiocarbon ages can be compared with OM radiocarbon ages at the same depth to establish simplified DCF corrections. These corrections can be applied to other CaCO_3 ages with no corresponding OM age, with correction values taken from paired samples that are closest and share a similar petrographic fabric.

Major differences in stalagmite petrography often signify changed environmental conditions (Railsback et al., 2013). Likewise, sections of BZBT1 with similar petrography are more likely to share similar environmental backgrounds and thus more similar DCF. Two major petrographic fabrics exist in BZBT1, and different DCF corrections are applied to these fabrics (Section S2, available online). In applying a simple DCF correction from one paired sample to other nearby CaCO_3 samples, we acknowledge that the actual DCF likely differs and the age estimate uncertainty

is higher than corrected CaCO_3 error bars suggest. While more sophisticated methods of correcting stalagmite CaCO_3 for DCF exist (e.g. Hua et al., 2012; Lechleitner et al., 2016b), these require higher quality chronological and environmental data than available with BZBT1. Thus, the simple transfer of age difference between the paired OM/ CaCO_3 ages is suitable for the initial approximate chronology, with the caveat that the corrected ages have wide uncertainty.

Linear age–depth models

Careful examination of the calibrated OM and U-Th age data in Figure 4 revealed that a single straight line (line AB in Figure 4) can be drawn that intersects three calibrated OM ages (OE1-3, OE1-4, and OE1-6) and three U-Th ages (U1-3, U1-4, and U1-8). Of the U-Th ages that intersect line AB, two have higher ^{238}U levels, one has low ^{232}Th , and all three have both fairly high $^{230}\text{Th}/^{232}\text{Th}$ ratios and lower age uncertainties (Table S1, available online). This line also falls within 150 years of one other OM age (OE1-1) and two other U-Th ages (U1-2 and U1-6). This line is therefore our initial age model for BZBT1 growth in the basal 73 mm of the stalagmite. If the OM we dated was aged prior to inclusion (i.e. not modern, as assumed), this line would need to be moved to the left. However, the slope of the line would likely not change substantially.

Assuming that the OM radiocarbon ages reflect the accurate age of deposition, we can use paired OM/ CaCO_3 uncalibrated radiocarbon ages at 20/21, 52/57, and 93/93 mm to estimate the ^{14}C year offset. The two upper age pairs come from the braided

calcite zone of BZBT1, while the lowest pairing comes from the dense calcite basal zone. The uppermost and middle age pairs have CaCO_3 ^{14}C ages that are 710 and 840 years older than the OM ^{14}C ages, respectively. These offsets are 700 and 800 years, respectively, if adjusted for the slight depth differences between the paired samples.

The lowest CaCO_3 sample is 310 and 390 years older than the two OM ages for this depth. This suggests that the DCF of the dense basal calcite is lower than the calcite in the upper braided section. A different DCF is not unexpected as petrography shows that the depositional environment was clearly different between the basal and upper sections. In addition, the isotopic values in this section are high, suggesting drier conditions, and drier conditions are associated with more closed hydrological systems and lower DCFs (Fohlmeister et al., 2010; Griffiths et al., 2012; Lechleitner et al., 2016a).

To correct and calibrate the CaCO_3 radiocarbon ages at 78, 80, and 88.5 mm, we used the dead carbon offset of 350 ^{14}C years averaged from the paired OM/ CaCO_3 ages at 93 mm. The corrected CaCO_3 ages from this lower section are 1470 ± 50 , 1250 ± 50 , and 1430 ± 50 ^{14}C yr BP, and the 2σ calibrated age ranges are 1292–1519 (median: 1363), 1066–1282 (median: 1192), and 1272–1412 (median: 1335) yr BP, respectively. Although the age ranges skew younger than our age model AB, they either overlap or are less than 150 years from this line. Knowing that the DCF likely varied through this section and that later tuning may shift our initial age model, we do not consider this slight age estimation offset to be significant.

While we do not have OM radiocarbon or robust U-Th ages for the top 17 mm of BZBT1, we do have two robust CaCO_3 radiocarbon ages (RC1-11 and RC1-9) at depths of 3 and 8 mm. We applied the average DCF correction of 750 ^{14}C years from the upper two paired OM/ CaCO_3 ages, as these are nearest to the two uppermost uncorrected CaCO_3 ages and also come from a zone with a similar braided calcite fabric. This produced corrected radiocarbon ages of 405 ± 50 and 585 ± 40 ^{14}C yr BP for 3 and 8 mm, respectively, and calibrating these ages provides us with 2σ calendar age ranges of 316–525 (median: 455) yr BP at 3 mm and 532–653 (median: 601) yr BP at 8 mm. By considering these new calibrated ages, as well as the U-Th age at 17 mm (U1-8), we derived linear growth line BC in Figure 4.

Our complete initial radiometric age–depth model for BZBT1 combines the lower line AB with the upper line BC. Worldwide, stalagmites largely grow between 0.01 and 1 mm/yr with a median growth rate of 0.1 mm/yr (Railsback, 2018). Four regional stalagmites (Akers et al., 2016; Kennett et al., 2012; Medina-Elizalde et al., 2010, 2016) grew between 0.13 and 0.30 mm/yr, with an average rate of 0.18 mm/yr. Our radiometric age–depth model indicates a reasonable, though slightly slow for the region, growth rate of 0.11 mm/yr for the main growth of BZBT1 below 20 mm.

The upper section of BZBT1 grew at a rate of 0.04 mm/yr, which is slower than other regional stalagmites. However, the isotopes and unusual petrography of this section support abnormal growth and a drying drip source which would help explain the slow growth. Beyond this simple model, petrographic evidence suggests that hiatuses and/or growth rate changes may be necessary for a truly accurate age–depth model in the upper 20 mm and lowest 13 mm of BZBT1 (Figure 4). However, as we lack the level of age precision to determine the duration or degree of such changes, we can only acknowledge their possible existence.

Minimum and maximum age constraints

Although we have strong reason to believe that the uppermost CaCO_3 and ^{210}Pb samples were contaminated with modern radioisotopes during sampling, the coincidence of both apex samples returning modern ages bears further examination. As a reminder,

the high modern carbon content of the uppermost CaCO_3 age sample is likely because of the inclusion of recent (<70 yr) post-bomb carbon, and ^{210}Pb activity dates the top 1 mm of BZBT1 to < 100 yr BP. However, steady sustained growth in the upper 20 mm to modern day seems unlikely. The resulting growth rate (~0.02 mm/yr) would be significantly lower than typically observed in stalagmites from similar environments (Railsback, 2018). At this rate, the 1–11 mm ^{210}Pb sample should contain deposits younger than 100 years and thus also have detectable activity; however, no activity was detected in this sample.

In addition, in order to reconcile the CaCO_3 ages at 3 and 8 mm with a predicted growth trend that supports a modern apex, the DCF correction would have to be 250 ^{14}C years greater in the top 20 mm than estimated for the 20–80 mm section. Increased precipitation and a more open hydrological system can produce higher DCF values, but the petrography and stable isotope ratios from this section suggest drying conditions. With the existing doubts regarding the potential sampling contamination of the uppermost CaCO_3 and ^{210}Pb samples, we conclude that our model line BC remains the best radiometric estimate for the age–depth relationship in the top 20 cm of BZBT1.

The line BC predicts an age of ~400 yr BP at the stalagmite top, and this predicted final growth age is supported by the ^{210}Pb and CaCO_3 radiocarbon data (excluding the likely contaminated uppermost samples) which suggest that deposition below 1 mm is older than 100 years. Although the U-Th data have high uncertainty, no sample was dated younger than 1000 years and five ages have relatively tight clustering between 1000 and 1500 yr BP. The combined results of only relatively old ages from ^{210}Pb , CaCO_3 radiocarbon, and U-Th supports the radiometric model estimate that BZBT1 stopped growing several centuries before present.

Our radiometric model line AB predicts that growth of BZBT1 began around 1550 yr BP. This is supported by additional evidence from our dating results. The two basal OM radiocarbon ages for BZBT1 are from detritus that immediately predates CaCO_3 deposition. Their ages thus indicate that BZBT1 began to form no earlier than 1650 ± 100 yr BP and potentially decades later if the OM was previously aged and/or CaCO_3 deposition did not immediately occur. Although U-Th cannot provide as precise of a maximum age constraint, linear trends fit through the five most robust U-Th ages agree with the OM data and suggest growth of BZBT1 began after 2000 yr BP.

Chronological tuning with stable isotopes

By applying the radiometric age–depth model in Figure 4 to the stable isotope data, we constructed a time series of $\delta^{18}\text{O}$ and $\delta^{13}\text{C}$ for BZBT1 (Figure 5). We then tuned the radiometric chronology by comparing the BZBT1 isotope record with the two nearest stalagmite records: MC01 from Macal Chasm (Akers et al., 2016) and YOK-I from Yok Balum (Kennett et al., 2012), which are approximately 30 and 90 km from Box Tunich, respectively. The MC01 record is constrained by 16 U-Th dates and contains 660 $\delta^{18}\text{O}$ and $\delta^{13}\text{C}$ data points spanning the last 5250 years, while the YOK-I record is constrained by 40 U-Th dates and contains ~4000 $\delta^{18}\text{O}$ and $\delta^{13}\text{C}$ data points spanning the last 2000 years (note that isotope samples younger than 100 yr BP for YOK-I are considered unreliable by Kennett et al.). The MC01 and YOK-I records have themselves been correlated with parallel sequences from a variety of paleoenvironmental sources across Mesoamerica as well as archaeological records and historic data (e.g. Akers et al., 2016; Bhattacharya et al., 2017; Ebert et al., 2017; Hoggarth et al., 2017; Kennett and Beach, 2013; Kennett et al., 2012).

For both MC01 and YOK-I, higher $\delta^{18}\text{O}$ and $\delta^{13}\text{C}$ values are inferred to reflect drier conditions as with BZBT1. We selected

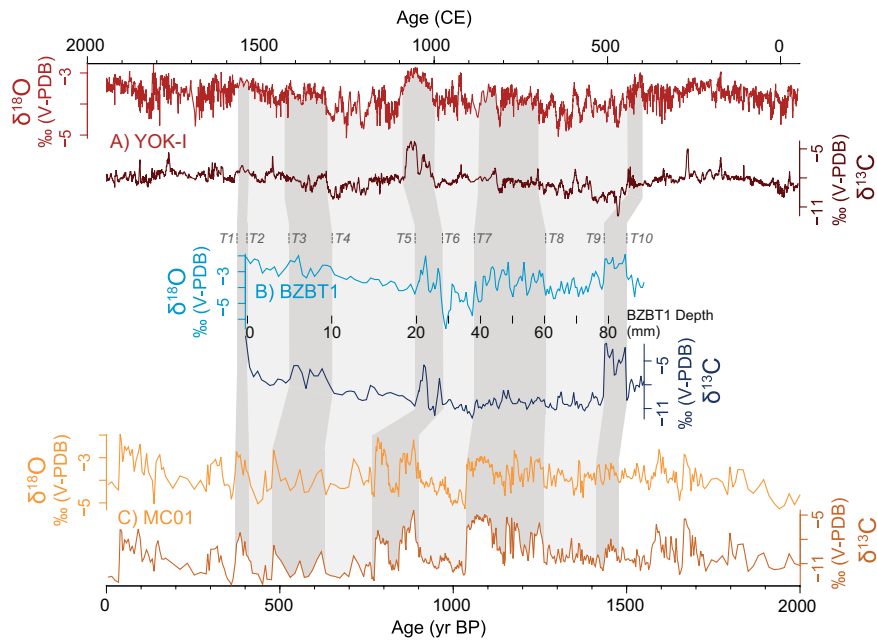


Figure 5. Values of $\delta^{18}\text{O}$ and $\delta^{13}\text{C}$ for stalagmites YOK-I (A) (Kennett et al., 2012), BZBT1 (B) (this study), and MC01 (C) (Akers et al., 2016). The BZBT1 data are plotted on the x-axis using the initial radiometric age–depth model. Tuning points are labeled *T1–T10* and intervening periods are highlighted by shading.

Table 1. Ages for matched isotope tuning points in the BZBT1, YOK-I, and MC01 records.

Tuning point	BZBT1 depth (mm)	BZBT1 age (radiometric chronology, yr BP)	YOK-I age (yr BP)	MC01 age (yr BP)
1	–	380	395	370
2	0	405	420	410
3	5	525	515	480
4	10	650	640	625
5	20	890	860	770
6	28	975	960	900
7	38	1060	1090	1040
8	60	1265	1255	1260
9	79	1430	1500	1410
10	86	1500	1550	1475

10 tuning points that divide the BZBT1 isotope record into nine periods. By comparing the isotopic values and patterns of these periods with the MC01 and YOK-I records, we identified parallel sequences between all three records and assigned ages to the tuning points (Table 1, Figure 5). Since MC01 has much greater age uncertainty than YOK-I, we consider the YOK-I tuning to be the most chronologically accurate. These matches were identified visually, as more advanced statistical identification for tuning between stalagmites is difficult because of differences in sample resolution and age uncertainty between the records.

The clearest match between the three records is the double peak of $\delta^{18}\text{O}$ and $\delta^{13}\text{C}$ located between 20 and 28 mm in BZBT1 (tuning points *T5* and *T6*). A similar double peak also appears in the YOK-I and MC01 records around 800–1000 yr BP. Although the YOK-I $\delta^{18}\text{O}$ values form a single, extended peak, the $\delta^{13}\text{C}$ data clearly show a double peak at this time. In addition, the closest match for the actual values of the $\delta^{18}\text{O}$ and $\delta^{13}\text{C}$ maxima in BZBT1's double peak ($>3\text{‰}$ and $>6\text{‰}$, respectively) are also found in the parallel double peaks of MC01 and YOK-I. The age offset between YOK-I and MC01 for the double peak is likely because of MC01's greater age uncertainty.

Low isotope values (particularly in $\delta^{18}\text{O}$) are observed preceding this double peak (*T6* and *T7*). The extreme low $\delta^{18}\text{O}$ values in BZBT1 during this interval are very similar to the MC01 record, where near-minimal $\delta^{18}\text{O}$ values also immediately precede its double peak maximum. In YOK-I, the period preceding the double peak has stable isotope values at a relative minimum within the period 800–1100 yr BP, although not as extremely low as with BZBT1 and MC01. BZBT1 also has an extended period of higher $\delta^{18}\text{O}$ values between 38 and 60 mm (*T7* and *T8*), which best matches the higher $\delta^{18}\text{O}$ values in MC01 and YOK-I associated with late Classic Maya droughts between 1050 and 1250 yr BP.

For the four tuning points bracketing these three well-matched periods (*T5–T8*), the initial radiometric age estimates for BZBT1 only differ on average from the YOK-I and MC01 ages by 21 and 55 years, respectively. Identification of the remaining tuning point matches is less certain because of less extreme isotope variance and more complex petrography in these periods, but the age data still constrain tuning possibilities here. For example, the high isotopic values between 80 and 87 mm (*T9* and *T10*) possibly appear to match with high values associated with the end of the Preclassic Period (1700–1800 yr BP) in YOK-I and MC01 (note that Akers et al. (2016) identify their age–depth model for this event in MC01 as a century too young). The OM radiocarbon ages from the base of BZBT1, however, set the maximum age of growth initiation to 1650 ± 100 yr BP. Assuming that the 5 mm between the base and the 80–87 mm section took at least a few decades to grow (consistent with other growth rates of BZBT1), this excludes a match with the Preclassic event.

The resulting BZBT1 age models tuned using YOK-I and MC01 are both very similar to the original, untuned radiometric age model (Figure 4). The tuned model based on the chronologically precise YOK-I record is especially similar in timing to the initial radiometric age estimates for BZBT1. Although a close agreement between the tuned and original models is not unexpected, the average magnitude of change from tuning with YOK-I and MC01 is only 26 and 35 years, respectively, and the largest individual age tune is 70 and 120 years, respectively. This supports the basic accuracy of the original radiometric age model we developed for BZBT1.

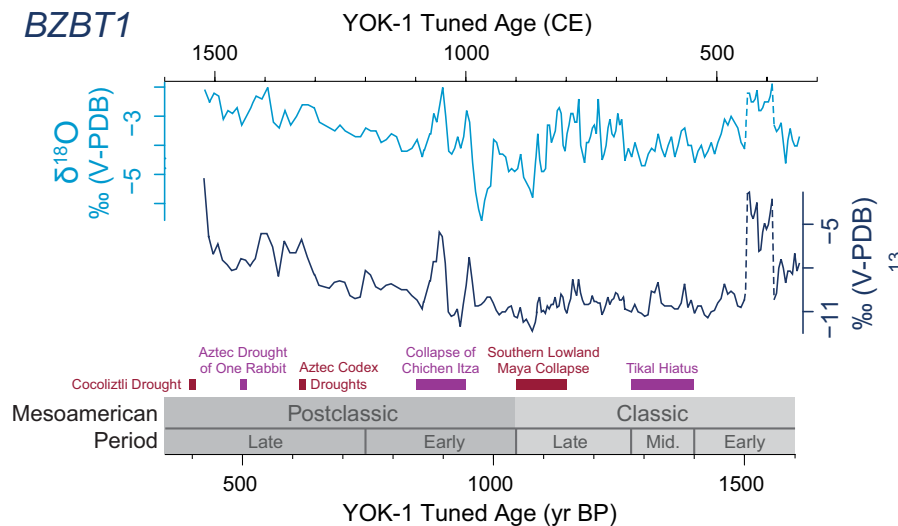


Figure 6. BZBT1 stable isotope record plotted using the isotope tuned age-depth model based on YOK-1 (Kennett et al., 2012). Mesoamerican chronological periods based on Vaca Plateau polity history (Iannone et al., 2014; Schwake and Iannone, 2016) are labeled at bottom, and significant droughts, famines, and political collapses are identified (Hoggarth et al., 2016; Iannone, 2014; Stahle et al., 2011; Therrell et al., 2004). Possible depositional interruptions in the Early Classic (Section S2, available online) are represented by dashed lines.

Paleoenvironmental implications of BZBT1

The age model tuned to YOK-1 is likely the most accurate chronology for BZBT1; therefore, ages listed in this section are derived from that model. While the tuning would seemingly prevent us from using BZBT1 as a wholly independent climate record, our original radiometric age model did not require substantial revision or shifting with the isotope tuning. Thus, our data independently support the following record of environmental change during Maya occupation. The early growth of BZBT1 occurs during a period of near-maximum regional population and land use intensity prior to the destabilization of Classic Maya society at the end of the Classic Period. As a result, many or most of the residential structures and terraces identified by the lidar analysis (Figure 1, S1, available online) would likely have been in use when BZBT1 began growing.

Five periods in the BZBT1 record have relatively higher isotope values (Figure 5) indicating drier conditions. These dry periods generally coincide with major dry events reported from other paleoenvironmental records across Mesoamerica (e.g. Akers et al., 2016), suggesting that these regionally reported droughts also affected Maya in the Belize River Valley. The droughts recorded by BZBT1 also coincide with several periods of social disruption, famine, and collapse across the Maya world (Figure 6).

The first dry period in BZBT1 occurs at the end of the early Classic Period from 1500 to 1560 yr BP (390–450 CE). Unlike later proposed dry periods in BZBT1, this does not coincide with any reported regional droughts. However, the high stable isotopes during this time come from layers of BZBT1 with a different, denser petrography, possible bracketing hiatuses, and potentially higher kinetic fractionation (Section S2, available online). As such, this extreme isotope excursion may be related more to changing, irregular CaCO_3 depositional patterns at the start of BZBT1's growth than an actual record of an extreme drought. Alternatively, the high isotopic values may indeed reflect an intense, localized drought not recorded in regional records.

BZBT1 records no major drought during the Tikal Hiatus, a multi-decadal absence of dedicated monuments in the city of Tikal precipitated by a major defeat in 562 CE at the hands of Caracol and Calakmul (Aimers and Iannone, 2014; Chase and Chase, 2003; Martin and Grube, 2008). However, the Tikal Hiatus

itself was largely restricted to Tikal, and its rivals (including Caracol in the Vaca Plateau) thrived during this time (Aimers and Iannone, 2014; Dahlin and Chase, 2014). A lack of drought here is not unexpected, as the Tikal Hiatus seems to have been primarily driven and shaped by socio-political forces, and other regional records generally show no major drought at this time as well.

Settlement histories at Belize River Valley sites show diverse trajectories during the early growth of BZBT1, with populations at some centers (e.g. Barton Ramie, Baking Pot, Pacbitun) growing between the early and late Classic Periods (Healy et al., 2007; Hoggarth, 2012; Willey et al., 1965). However, Xunantunich, Actuncan, and Buenavista del Cayo exhibit evidence for population decline or stagnation in the transition from the early to late Classic Period (Mixer, 2016; Peuramaki-Brown, 2012; Yaeger, 2008). Based on the relatively stable climate suggested by BZBT1 in the middle Classic, these different trajectories are more likely rooted in varied responses, adaptations, and impacts from changing socio-economic conditions than adverse drought across the region.

The well-documented collapse of Southern Lowland Maya polities coincides with the latter phase of an extended period of cyclical droughts recorded in BZBT1 between 1090 and 1255 yr BP (695–860 CE). The environmental pressure from extended and repeated drought may have led to the increased regional warfare at this time (Akers et al., 2016; Iannone, 2014; Martin and Grube, 2008), and the small communities in the karst upland near BZBT1 would have been significantly stressed by their socio-environmental setting. By the end of this period, the ruling dynasties living at major population centers of western Belize and the neighboring Petén region of Guatemala (including Caracol and Tikal) disintegrated and the region was depopulated, likely as a result of societal destabilization in the face of drought and conflict.

After a century-long reprieve of very wet conditions, extreme drought returned in a twin-peaked event at 860–960 yr BP (990–1090 CE). The collapse of Chichen Itza and most of the Northern Lowland Maya polities occurred during this early Postclassic drought (Hoggarth et al., 2016), and hiatuses in activity are observed in the Belize River Valley as well (Hoggarth et al., 2014). It is likely that most remnant population centers in the Belize River Valley would also have been significantly affected and possibly depopulated during this very severe event.

Although the BZBT1 chronology is not as constrained in the upper 20 mm, two periods of drier conditions are intriguingly

close in timing to droughts and famines recorded in Aztec codices. While those codices recorded events in locations 1000 km west of Box Tunich, widespread drought caused by shifts in ITCZ position, monsoonal strength, and/or Atlantic and Pacific oceanic forcings are often expressed broadly across Mesoamerica (e.g. Akers et al., 2016; Bhattacharya et al., 2015, 2017; Stahle et al., 2011). Drought-driven famine recorded in Aztec codices during the 1330s and 1450s CE, including the particularly severe Famine of One Rabbit in 1454 CE (Therrell et al., 2004), may be reflected in the higher isotope values in BZBT1 between 500 and 650 yr BP (1300–1450 CE).

Finally, our age model estimates that BZBT1 stopped growing shortly before 400 yr BP, and this coincides with a severe drought well-documented in the mid-16th century CE in central Mexico for its associated cocoliztli epidemics and population collapse (Acuna-Soto et al., 2002; Hunt and Elliott, 2002; Stahle et al., 2000, 2011). Historic records in northern Yucatan also document a severe drought across the Yucatan peninsula in 1535–1541 CE that affected agricultural production and contributed to high mortality (Hoggarth et al., 2017). While the drip source feeding BZBT1 appears to have been slowing for several centuries, this severe drought may have triggered its final drying and closing.

It is possible that a change in land use above Box Tunich, such as clearing for agricultural expansion in response to population growth in the Classic Period, triggered the initial growth of BZBT1 (or the transition from dense to braided calcite fabric at 80 mm) by altering water infiltration and soil characteristics to favor stalagmite growth. In this manner, regional land abandonment and forest recovery in the Postclassic Period may have led to the growth slowing and/or the change to irregular laminae in the upper 20 mm as the environment returned to more natural conditions that were unfavorable to BZBT1's growth. While this hypothesis is speculative and difficult to verify in the absence of more precise dates for both BZBT1 and the regional land use history, it would help explain the otherwise serendipitous coincidence that our relatively short stalagmite record overlaps so well with Classic Maya history.

Conclusion

Through the combined evidence from four radiometric dating methods and stable isotope tuning, we are able to propose that BZBT1 grew between 400 and 1610 yr BP. Although the age estimation from each individual dating method is inconclusive, an independent radiometric age model can be constructed from their combined data. This dating of BZBT1 is significant in that it allows useful paleoenvironmental analysis of a specimen that would traditionally be considered 'undatable' and ignored. Instead, we have shown that the severe dry events of the late Classic and early Preclassic Periods observed across Mesoamerica also impacted the Belize River Valley. As archaeological research continues in this region, it is likely that additional paleoclimate records will be desired, and our work can help plan for more successful climate reconstructions from speleothems.

Based on our regional speleothem sampling in western Belize and discussions with other paleoclimatologists working in the region, low uranium concentrations should be assumed for any stalagmite collected in the Belize River Valley and on the Vaca Plateau. Ideally, stalagmites identified for potential sampling should be pre-screened for uranium content, and specimen sampling should target aragonite stalagmites if possible. In this manner, a stalagmite suitable for traditional U-Th dating may be found and alternative means of dating need not be used.

If no suitable stalagmite can be found for U-Th dating, or if the paleoclimate value of a specific speleothem intrinsically makes it difficult to date by U-Th methods (e.g. flowstone cores

or stalagmites bearing flood deposits), then our described methods for dating BZBT1 may be helpful. Further reductions in age estimation uncertainty can be achieved through additional field sampling of other materials along with the targeted speleothem. In particular, thorough sampling of soils above and within the cave can help greatly in constraining the assumed OM age needed for radiocarbon dating of trapped OM. By attempting OM radiocarbon dating on more stalagmites that have been successfully dated by U-Th, we may also better learn about the sourcing and flux of OM input in cave systems.

As the field of speleothem paleoclimatology continues to expand, the increasing demand for scientific specimens presents a serious ethical and conservation challenge for the finite supply of speleothems. Rather than collecting new stalagmites for every project and taking several stalagmites to increase the chance of a successful specimen, we should instead re-examine the potential of stalagmites previously collected and currently archived. Since many of these stalagmites are likely archived because of dating difficulties, alternative dating techniques offer the potential to extract important paleoenvironmental information without further impact on caves. Thus, alternatives to dating speleothems beyond traditional U-Th methods may prove critical in enabling the field of speleothem paleoclimatology to continue its growth well into a sustainable future.

Acknowledgements

We thank Jason S. Polk, Ben Miller, Jim Webster, Phil Reeder, Bill Reynolds, and Madeline Reynolds for assistance in the field. We also express our gratitude to the Belize Institute of Archaeology for their support of this project. Finally, we thank two reviewers for their very helpful comments and suggestions in improving this manuscript.


Funding

This research was funded by the Alphawood Foundation.

Supplemental material

Supplemental material for this article is available online.

ORCID iD

Pete Douglas Akers  <https://orcid.org/0000-0002-2266-5551>

References

- Acuna-Soto R, Stahle DW, Cleaveland MK et al. (2002) Megadrought and megadeath in 16th century Mexico. *Emerging Infectious Diseases* 8: 360–362.
- Adkins JF, Carolin SA, Cobb KM et al. (2013) U-series dating of tropical stalagmites. In: *American Geophysical Union, Fall Meeting*, San Francisco, CA, 9–13 December.
- Aimers JJ (2007) What Maya collapse? Terminal classic variation in the Maya lowlands. *Journal of Archaeological Research* 15: 329–377.
- Aimers JJ and Iannone G (2014) The dynamics of ancient Maya developmental history. In: Iannone G (ed.) *The Great Maya Droughts in Cultural Context: Case Studies in Resilience and Vulnerability*. Boulder, CO: University Press of Colorado, pp. 21–49.
- Akers PD (2011) *Climate and Maya cultural change: Detecting connections using Belizean stalagmites*. MS Thesis, Department of Geography, University of Georgia, Athens, GA.
- Akers PD (2016) *Paleoclimate change in southern Indiana determined from speleothem climate proxies and analysis of modern precipitation oxygen isotope variations*. Doctoral Dissertation, Department of Geography, University of Georgia, Athens, GA.

- Akers PD, Brook GA, Railsback LB et al. (2016) An extended and higher-resolution record of climate and land use from stalagmite MC01 from Macal Chasm, Belize, revealing connections between major dry events, overall climate variability, and Maya sociopolitical changes. *Palaeogeography, Palaeoclimatology, Palaeoecology* 459: 268–288.
- Appleby PG (1998) Dating recent sediments by Pb-210: Problems and solutions. In: *Proceedings of a Seminar*, Helsinki, 2–3 April, 1997, pp. 7–24. Helsinki: Finland Radiation and Nuclear Safety Authority.
- Appleby PG, Shotyk W and Fankhauser A (1997) Lead-210 age dating of three peat cores in the Jura mountains, Switzerland. *Water Air and Soil Pollution* 100: 223–231.
- Awe JJ, Hoggarth JA and Helmke C (2014) Prehistoric settlement patterns in the Upper Belize River Valley and their implications for models of low-density urbanism. *Acta Mesoamericana* 27: 263–285.
- Bajo P, Hellstrom J, Frisia S et al. (2016) ‘Cryptic’ diagenesis and its implications for speleothem geochronologies. *Quaternary Science Reviews* 148: 17–28.
- Banner JL, Guilfoyle A, James EW et al. (2007) Seasonal variations in modern speleothem calcite growth in Central Texas, USA. *Journal of Sedimentary Research* 77: 615–622.
- Baskaran M and Iliffe TM (1993) Age determination of recent cave deposits using excess ^{210}Pb – A new technique. *Geophysical Research Letters* 20: 603–606.
- Bhattacharya T, Byrne R, Bohnel H et al. (2015) Cultural implications of Late-Holocene climate change in the Cuenca Oriental, Mexico. *Proceedings of the National Academy of Sciences of the United States of America* 112: 1693–1698.
- Bhattacharya T, Chiang JCH and Cheng W (2017) Ocean-atmosphere dynamics linked to 800–1050 CE drying in Mesoamerica. *Quaternary Science Reviews* 169: 263–277.
- Blyth AJ, Hartland A and Baker A (2016) Organic proxies in speleothems – New developments, advantages and limitations. *Quaternary Science Reviews* 149: 1–17.
- Blyth AJ, Hua Q, Smith A et al. (2017) Exploring the dating of ‘dirty’ speleothems and cave sinters using radiocarbon dating of preserved organic matter. *Quaternary Geochronology* 39: 92–98.
- Borsato A, Frisia S and Miorandi R (2015) Carbon dioxide concentration in temperate climate caves and parent soils over an altitudinal gradient and its influence on speleothem growth and fabrics. *Earth Surface Processes and Landforms* 40: 1158–1170.
- Borsato A, Frisia S, Jones B et al. (2000) Calcite moonmilk: Crystal morphology and environment of formation in caves in the Italian Alps. *Journal of Sedimentary Research* 70: 1171–1182.
- Broecker WS, Olson EA and Orr PC (1960) Radiocarbon measurements and annual rings in cave formations. *Nature* 185: 93–94.
- Brook GA, Cherkinsky A, Railsback LB et al. (2013) ^{14}C dating of organic residue and carbonate from stromatolites in Etosha Pan, Namibia: ^{14}C reservoir effect, correction of published ages, and evidence of >8-m-deep lake during the Late Pleistocene. *Radiocarbon* 55: 1156–1163.
- Cai YJ, Beck W, Peng ZC et al. (2005) Effect of dead carbon on the ^{14}C dating of the speleothem. *Chinese Science Bulletin* 50: 817–821.
- Chase AF and Chase DZ (2007) ‘This is the End’: Archaeological transitions and the terminal classic period at Caracol, Belize. *Research Reports in Belizean Archaeology* 4: 13–27.
- Chase DZ and Chase AF (2003) Texts and contexts in classic Maya warfare: A brief consideration of epigraphy and archaeology at Caracol, Belize. In: Brown MK and Stanton T (eds) *Ancient Mesoamerican Warfare*. Walnut Creek, CA: Alta Mira Press, pp. 171–188.
- Chase AF, Chase DZ, Awe JJ et al. (2014) Ancient Maya regional settlement and inter-site analysis: The 2013 west-central Belize LiDAR survey. *Remote Sensing* 6: 8671–8695.
- Cheng H, Edwards RL, Hoff J et al. (2000) The half-lives of uranium-234 and thorium-230. *Chemical Geology* 169: 17–33.
- Czaplewski NJ, Krejca J and Miller TE (2003) Late quaternary bats from Cebada Cave, Chiquibul cave system, Belize. *Caribbean Journal of Science* 39: 23–33.
- Dahlin BH and Chase AF (2014) A tale of three cities: Effects of the A.D. 536 in the Lowland Maya heartland. In: Iannone G (ed.) *The Great Maya Droughts in Cultural Context: Case Studies in Resilience and Vulnerability*. Boulder, CO: University Press of Colorado, pp. 127–155.
- Denniston RF and Luetscher M (2017) Speleothems as high-resolution paleoflood archives. *Quaternary Science Reviews* 170: 1–13.
- Denniston RF, González LA, Asmerom Y et al. (1999) Evidence for increased cool season moisture during the middle Holocene. *Geology* 27: 815–818.
- Dorale JA, Edwards RL, Alexander EC et al. (2004) Uranium-series dating of speleothems: Current techniques, limits, & applications. In: Sasowsky ID and Mylroie J (eds) *Studies of Cave Sediments: Physical and Chemical Records of Paleoclimate*. Boston, MA: Springer, pp. 177–197.
- Douglas PMJ, Brenner M and Curtis JH (2016) Methods and future directions for paleoclimatology in the Maya Lowlands. *Global and Planetary Change* 138: 3–24.
- Dreybrodt W and Scholz D (2011) Climatic dependence of stable carbon and oxygen isotope signals recorded in speleothems: From soil water to speleothem calcite. *Geochimica et Cosmochimica Acta* 75: 734–752.
- Drysdale RN, Zanchetta G, Hellstrom JC et al. (2007) Stalagmite evidence for the precise timing of North Atlantic cold events during the early last glacial. *Geology* 35: 77–80.
- Ebert CE, Hoggarth JA and Awe JJ (2016) Integrating quantitative lidar analysis and settlement survey in the Belize River Valley. *Advances in Archaeological Practice* 4: 284–300.
- Ebert CE, Peniche-May N, Culleton BJ et al. (2017) Regional response to drought during the formation and decline of pre-classic Maya societies. *Quaternary Science Reviews* 173: 211–235.
- Ebert CE, Prufer KM, Macri MJ et al. (2014) Terminal long count dates and the disintegration of classic period Maya polities. *Ancient Mesoamerica* 25: 337–356.
- Edwards RL, Chen JH and Wasserburg GJ (1987) U-238-U-234-TH-230-TH-232 systematics and the precise measurement of time over the past 500,000 years. *Earth and Planetary Science Letters* 81: 175–192.
- Fairchild IJ and Baker A (2012) *Speleothem Science: From Process to past Environments*. Chichester: John Wiley & Sons.
- Farquhar GD, Ehleringer JR and Hubick KT (1989) Carbon isotope discrimination and photosynthesis. *Annual Review of Plant Physiology and Plant Molecular Biology* 40: 503–537.
- Fensterer C, Scholz D, Hoffmann D et al. (2010) $^{230}\text{Th}/\text{U}$ -dating of a late Holocene low uranium speleothem from Cuba. In: *Pages 1st Young Scientists Meeting*, Corvallis, OR, 6–7 July 2009. Bristol: IOP Publishing.
- Fohlmeister J, Schroder-Ritzrau A, Spotl C et al. (2010) The influences of hydrology on the radiogenic and stable carbon isotope composition of cave drip water, Grotta di Ernesto (Italy). *Radiocarbon* 52: 1529–1544.
- Genty D, Blamart D, Ouahdi R et al. (2003) Precise dating of Dansgaard-Oeschger climate oscillations in western Europe from stalagmite data. *Nature* 421: 833.

- Genty D, Konik S, Valladas H et al. (2011) Dating the Lascaux Cave Gour formation. *Radiocarbon* 53: 479–500.
- Genty D, Massault M, Gilmour M et al. (1999) Calculation of past dead carbon proportion and variability by the comparison of AMS(14)C and TIMS U/Th ages on two holocene stalagmites. *Radiocarbon* 41: 251–270.
- Genty D, Vokal B, Obelic B et al. (1998) Bomb C-14 time history recorded in two modern stalagmites – Importance for soil organic matter dynamics and bomb C-14 distribution over continents. *Earth and Planetary Science Letters* 160: 795–809.
- Goslar T, Hercman H and Pazdur A (2000) Comparison of U-series and radiocarbon dates of speleothems. *Radiocarbon* 42: 403–414.
- Griffiths ML, Fohlmeister J, Drysdale RN et al. (2012) Hydrological control of the dead carbon fraction in a Holocene tropical speleothem. *Quaternary Geochronology* 14: 81–93.
- Hartmann A and Baker A (2017) Modelling karst vadose zone hydrology and its relevance for paleoclimate reconstruction. *Earth-Science Reviews* 172: 178–192.
- Haug GH, Gunther D, Peterson LC et al. (2003) Climate and the collapse of Maya civilization. *Science* 299: 1731–1735.
- Healy PF, Helmke CGB, Awe JJ et al. (2007) Survey, settlement, and population history at the ancient Maya site of Pacbitun, Belize. *Journal of Field Archaeology* 32: 17–39.
- Hellstrom J and Pickering R (2015) Recent advances and future prospects of the U-Th and U-Pb chronometers applicable to archaeology. *Journal of Archaeological Science* 56: 32–40.
- Hendy CH and Wilson AT (1968) Palaeoclimatic data from speleothems. *Nature* 219: 48–51.
- Hodell DA, Brenner M and Curtis JH (2005) Terminal classic drought in the northern Maya lowlands inferred from multiple sediment cores in Lake Chichancanab (Mexico). *Quaternary Science Reviews* 24: 1413–1427.
- Hodge E, McDonald J, Fischer M et al. (2011) Using the C-14 bomb pulse to date young speleothems. *Radiocarbon* 53: 345–357.
- Hoggarth JA (2012) *Social reorganization and household adaptation in the aftermath of collapse at Baking Pot, Belize*. PhD Dissertation, University of Pittsburgh, Pittsburgh, PA.
- Hoggarth JA, Breitenbach SFM, Culleton BJ et al. (2016) The political collapse of Chichén Itzá in climatic and cultural context. *Global and Planetary Change* 138: 25–42.
- Hoggarth JA, Culleton BJ, Awe JJ et al. (2014) Questioning post-classic continuity at Baking Pot, Belize, using direct AMS 14C dating of human burials. *Radiocarbon* 56: 1057–1075.
- Hoggarth JA, Restall M, Wood JW et al. (2017) Drought and its demographic effects in the Maya Lowlands. *Current Anthropology* 58: 82–113.
- Hua Q, McDonald J, Redwood D et al. (2012) Robust chronological reconstruction for young speleothems using radiocarbon. *Quaternary Geochronology* 14: 67–80.
- Hunt B and Elliott T (2002) Mexican megadrought. *Climate Dynamics* 20: 1–12.
- Iannone G (2014) *The Great Maya Droughts in Cultural Context: Case Studies in Resilience and Vulnerability*. Boulder, CO: University Press of Colorado.
- Iannone G, Chase AF, Chase DZ et al. (2014) An archaeological consideration of long-term socio-ecological dynamics on the Vaca Plateau, Belize. In: Iannone G (ed.) *The Great Maya Droughts in Cultural Context: Case Studies in Resilience and Vulnerability*. Boulder, CO: University Press of Colorado, pp. 271–300.
- Jamieson RA, Baldini JUL, Brett MJ et al. (2016) Intra- and inter-annual uranium concentration variability in a Belizean stalagmite controlled by prior aragonite precipitation: A new tool for reconstructing hydro-climate using aragonitic speleothems. *Geochimica et Cosmochimica Acta* 190: 332–346.
- Kennett DJ and Beach TP (2013) Archeological and environmental lessons for the Anthropocene from the Classic Maya collapse. *Anthropocene* 4: 88–100.
- Kennett DJ, Breitenbach SFM, Aquino VV et al. (2012) Development and disintegration of Maya political systems in response to climate change. *Science* 338: 788–791.
- Lachniet MS (2009) Climatic and environmental controls on speleothem oxygen-isotope values. *Quaternary Science Reviews* 28: 412–432.
- Lachniet MS, Bernal JP, Asmerom Y et al. (2012) Uranium loss and aragonite-calcite age discordance in a calcitized aragonite stalagmite. *Quaternary Geochronology* 14: 26–37.
- Lambert WJ and Aharon P (2011) Controls on dissolved inorganic carbon and delta C-13 in cave waters from DeSoto Caverns: Implications for speleothem delta C-13 assessments. *Geochimica et Cosmochimica Acta* 75: 753–768.
- Lechleitner FA, Baldini JUL, Breitenbach SFM et al. (2016a) Hydrological and climatological controls on radiocarbon concentrations in a tropical stalagmite. *Geochimica et Cosmochimica Acta* 194: 233–252.
- Lechleitner FA, Fohlmeister J, McIntyre C et al. (2016b) A novel approach for construction of radiocarbon-based chronologies for speleothems. *Quaternary Geochronology* 35: 54–66.
- Li J-Y, Li H-C, Li T-Y et al. (2017) High-resolution $\delta^{18}\text{O}$ and $\delta^{13}\text{C}$ records of an AMS 14C and 230Th/U dated stalagmite from Xinya Cave in Chongqing: Climate and vegetation change during the Late-Holocene. *Quaternary International* 447: 75–88.
- McDermott F (2004) Palaeo-climate reconstruction from stable isotope variations in speleothems: A review. *Quaternary Science Reviews* 23: 901–918.
- McGarry SF and Baker A (2000) Organic acid fluorescence: Applications to speleothem palaeoenvironmental reconstruction. *Quaternary Science Reviews* 19: 1087–1101.
- McGarry SF and Caseldine C (2004) Speleothem palynology: An undervalued tool in Quaternary studies. *Quaternary Science Reviews* 23: 2389–2404.
- Markowska M, Baker A, Andersen MS et al. (2016) Semi-arid zone caves: Evaporation and hydrological controls on $\delta^{18}\text{O}$ drip water composition and implications for speleothem paleoclimate reconstructions. *Quaternary Science Reviews* 131: 285–301.
- Martin S and Grube N (2008) *Chronicle of Maya Kings and Queens: Deciphering the Dynasties of the Ancient Maya*. 2nd Edition. London: Thames and Hudson.
- Martinson DG, Pisias NG, Hays JD et al. (1987) Age dating and the orbital theory of the ice ages: Development of a high-resolution 0 to 300,000-year chronostratigraphy. *Quaternary Research* 27: 1–29.
- Mattey DP, Fairchild IJ, Atkinson TC et al. (2010) Seasonal microclimate control of calcite fabrics, stable isotopes and trace elements in modern speleothem from St Michaels Cave, Gibraltar. In: Pedley HM and Rogerson M (eds) *Tufas and Speleothems: Unravelling the Microbial and Physical Controls*. London: Geological Society of London (Special Publications 336), pp. 323–344.
- Medina-Elizalde M and Rohling EJ (2012) Collapse of classic Maya civilization related to modest reduction in precipitation. *Science* 335: 956–959.
- Medina-Elizalde M, Burns SJ, Lea DW et al. (2010) High resolution stalagmite climate record from the Yucatán Peninsula spanning the Maya terminal classic period. *Earth and Planetary Science Letters* 298: 255–262.
- Medina-Elizalde M, Burns SJ, Polanco-Martínez JM et al. (2016) High-resolution speleothem record of precipitation from the Yucatan Peninsula spanning the Maya Preclassic Period. *Global and Planetary Change* 138: 93–102.

- Meyer KW, Feng WM, Breecker DO et al. (2014) Interpretation of speleothem calcite $\delta^{13}\text{C}$ variations: Evidence from monitoring soil CO_2 , drip water, and modern speleothem calcite in central Texas. *Geochimica Et Cosmochimica Acta* 142: 281–298.
- Mixter DW (2016) *Surviving collapse: Collective memory and political reorganization at Actuncan, Belize*. PhD Dissertation. Washington University, St. Louis.
- Moquet JS, Cruz FW, Novello VF et al. (2016) Calibration of speleothem $\delta^{18}\text{O}$ records against hydroclimate instrumental records in Central Brazil. *Global and Planetary Change* 139: 151–164.
- Noronha AL, Johnson KR, Hu CY et al. (2014) Assessing influences on speleothem dead carbon variability over the Holocene: Implications for speleothem-based radiocarbon calibration. *Earth and Planetary Science Letters* 394: 20–29.
- Noronha AL, Johnson KR, Southon JR et al. (2015) Radiocarbon evidence for decomposition of aged organic matter in the vadose zone as the main source of speleothem carbon. *Quaternary Science Reviews* 127: 37–47.
- O’Leary MH (1988) Carbon isotopes in photosynthesis. *Bioscience* 38: 328–336.
- Penn MG, Sutton DA and Monro A (2004) Vegetation of the greater Maya mountains, Belize. *Systematics and Biodiversity* 2: 21–44.
- Peuramaki-Brown M (2012) *The integration and disintegration of ancient Maya urban centres: Charting households and community at Buenavista del Cayo, Belize*. PhD Dissertation, University of Calgary, Calgary, AB, Canada.
- Polk JS, van Beynen PE and Reeder PP (2007) Late-Holocene environmental reconstruction using cave sediments from Belize. *Quaternary Research* 68: 53–63.
- Powers JS and Veldkamp E (2005) Regional variation in soil carbon and $\delta^{13}\text{C}$ in forests and pastures of northeastern Costa Rica. *Biogeochemistry* 72: 315–336.
- Pu J, Wang A, Shen L et al. (2016) Factors controlling the growth rate, carbon and oxygen isotope variation in modern calcite precipitation in a subtropical cave, Southwest China. *Journal of Asian Earth Sciences* 119: 167–178.
- Railsback LB (2018) A comparison of growth rate of Late-Holocene stalagmites with atmospheric precipitation and temperature, and its implications for paleoclimatology. *Quaternary Science Reviews* 187: 94–111.
- Railsback LB, Brook GA and Webster JW (1999) Petrology and paleoenvironmental significance of detrital sand and silt in a stalagmite from Drotsky’s Cave, Botswana. *Physical Geography* 20: 331–347.
- Railsback LB, Akers PD, Wang LX et al. (2013) Layer-bounding surfaces in stalagmites as keys to better paleoclimatological histories and chronologies. *International Journal of Speleology* 42: 167–180.
- Sanchez-Cabeza JA and Ruiz-Fernández AC (2012) 210Pb sediment radiochronology: An integrated formulation and classification of dating models. *Geochimica et Cosmochimica Acta* 82: 183–200.
- Schwake SA and Iannone G (2016) Destruction events and political truncation at the Little Kingdom of Minanha, Belize. In: Iannone G, Houk BA and Schwake SA (eds) *Ritual, Violence, and the Fall of the Classic Maya*. Gainesville, FL: University Press of Florida, pp. 134–158.
- Scroton N, Gagan MK, Dunbar GB et al. (2016) Natural attrition and growth frequency variations of stalagmites in southwest Sulawesi over the past 530,000 years. *Palaeogeography, Palaeoclimatology, Palaeoecology* 441: 823–833.
- Shackleton NJ (2000) The 100,000-year ice-age cycle identified and found to lag temperature, carbon dioxide, and orbital eccentricity. *Science* 289: 1897–1902.
- Shen CC, Edwards RL, Cheng H et al. (2002) Uranium and thorium isotopic and concentration measurements by magnetic sector inductively coupled plasma mass spectrometry. *Chemical Geology* 185: 165–178.
- Stahle DK, Cook ER, Cleaveland MK et al. (2000) Tree-ring data document 16th century megadrought over North America. *Eos, Transactions American Geophysical Union* 81: 121–125.
- Stahle DW, Diaz JV, Burnette DJ et al. (2011) Major Mesoamerican droughts of the past millennium. *Geophysical Research Letters* 38: L05703.
- Stuiver M and Reimer PJ (1993) Extended 14C data base and revised CALIB 3.0 14C age calibration program. *Radiocarbon* 35: 215–230.
- Tanahara A, Taira H, Yamakawa K et al. (1998) Application of excess Pb-210 dating method to stalactites. *Geochemical Journal* 32: 183–187.
- Therrell MD, Stahle DW and Soto RA (2004) Aztec drought and the ‘curse of one rabbit’. *Bulletin of the American Meteorological Society* 85: 1263.
- Trumbore S (2000) Age of soil organic matter and soil respiration: Radiocarbon constraints on belowground C dynamics. *Ecological Applications* 10: 399–411.
- Trumbore SE (1993) Comparison of carbon dynamics in tropical and temperate soils using radiocarbon measurements. *Global Biogeochemical Cycles* 7: 275–290.
- Turner BL and Sabloff JA (2012) Classic period collapse of the central Maya lowlands: Insights about human–environment relationships for sustainability. *Proceedings of the National Academy of Sciences of the United States of America* 109: 13908–13914.
- Vogel JS, Southon JR, Nelson DE et al. (1984) Performance of catalytically condensed carbon for use in accelerator mass spectrometry. *Nuclear Instruments and Methods in Physics Research* 5: 289–293.
- Wahl D, Byrne R and Anderson L (2014) An 8700 year paleoclimate reconstruction from the southern Maya lowlands. *Quaternary Science Reviews* 103: 19–25.
- Walling DE (1999) Linking land use, erosion and sediment yields in river basins. *Hydrobiologia* 410: 223–240.
- Wang YJ, Cheng H, Edwards RL et al. (2001) A high-resolution absolute-dated late pleistocene monsoon record from Hulu Cave, China. *Science* 294: 2345–2348.
- Wassenburg JA, Scholz D, Jochum KP et al. (2016) Determination of aragonite trace element distribution coefficients from speleothem calcite–aragonite transitions. *Geochimica et Cosmochimica Acta* 190: 347–367.
- Webster JW, Brook GA, Railsback LB et al. (2007) Stalagmite evidence from Belize indicating significant droughts at the time of preclassic abandonment, the Maya Hiatus, and the classic Maya collapse. *Palaeogeography, Palaeoclimatology, Palaeoecology* 250: 1–17.
- Westerhold T, Rohl U, Raffi I et al. (2008) Astronomical calibration of the Paleocene time. *Palaeogeography, Palaeoclimatology, Palaeoecology* 257: 377–403.
- Willey GR, Bullard Jr WR, Glass JB et al. (1965) *Prehistoric Maya settlements in the Belize Valley* (Papers of the Peabody Museum of Archaeology and Ethnology). Cambridge: Harvard University.
- Wong CI and Breecker DO (2015) Advancements in the use of speleothems as climate archives. *Quaternary Science Reviews* 127: 1–18.
- Woodhead J and Pickering R (2012) Beyond 500 ka: Progress and prospects in the UPb chronology of speleothems, and their application to studies in palaeoclimate, human evolution, biodiversity and tectonics. *Chemical Geology* 322–323: 290–299.
- Wynn PM and Brocks JJ (2014) A framework for the extraction and interpretation of organic molecules in speleothem carbonate. *Rapid Communications in Mass Spectrometry* 28: 845–854.
- Yaeger J (2008) Charting the collapse: Late classic to postclassic population dynamics in the Mopan valley, Belize. *Research Reports in Belizean Archaeology* 5: 13–21.